Available online at www.sciencedirect.com
SCIENCE DIRECT®
International Journal of Heat and Mass Transfer 49 (2006) 1264–1273
International Journal of HEAT and MASS TRANSFER
www.elsevier.com/locate/ijhmt

A non-linear approach for the analysis and modelling of the dynamics of systems exhibiting Vapotron effect

C. Biserni [a,*], A. Fichera [b], I.D. Guglielmino [b], E. Lorenzini [a], A. Pagano [b]

[a] *DIENCA, Università degli Studi di Bologna, Dipartimento di Ingegneria Energetica, Nucleare e del Controllo Ambientale, Viale Risorgimento 2, 40136 Bologna, Italy*

[b] *DIIM, Università di Catania, Dipartimento di Ingeneria Industriale e Meccanica, Viale Andrea Doria 6, 95125 Catania, Italy*

Received 21 January 2005; received in revised form 29 September 2005
Available online 9 December 2005

Abstract

This study presents a novel approach for the analysis of the experimental dynamical behaviour of a system exhibiting Vapotron effect. This phenomenon occurs as a subcooled boiling of a refrigerant fluid entrapped in the cavities of a non-isothermally heated finned surface. A preliminary characterisation of the experimental time series has been carried out to detect the existence of a low dimensional source of the dynamics, through the adoption of non-linear time series analysis techniques. In this way the existence of chaos has been observed in the system in study, which is therefore non-linear.

As a second step, a low-order non-linear model has been developed for the identification of the system dynamics. In particular, the NARMAX (Non-linear Auto-Regressive Moving Average with eXogenous inputs) identification strategy has been chosen for its flexibility, and has been implemented and generalised by means of Multilayer Perceptron neural networks. The neural model has been tested with satisfactory performances, showing the suitability of non-linear identification strategies as a reliable predictive tools for the dynamics of such kind of systems.

1. Introduction and phenomenology

The advance of several technological components, especially in the energetic and electronic [1,2] sectors, is subjected to the fulfilment of stringent requirements of compactness and growing heat power. Both these requirements strongly increase the heat density of modern components and impose the enhancement of appropriate heat removal technologies. Devices designed in order to promote boiling heat transfer have a great potential in this kind of applications, due to the high heat density that can be removed in presence of boiling phenomena. As well known, in order to avoid the burnout of the device, the maximum removable heat density usually coincides with the critical heat flux (CHF), or departure from nucleate boiling (DNB), which is etymologically the upper limit of the nucleate boiling regime. In other words, when the critical heat flux is exceeded, a sharp reduction of the local heat transfer coefficient causes a sudden rise in surface temperature, up to the above-mentioned burnout phenomenon. For practical applications in cooling systems, subcooled flow boiling of water is considered to be advantageous for the enhancement of heat removal. Several correlations and models for the evaluation of the CHF of subcooled flow boiling in water have been evaluated and compared in [3]. Some other examples of CHF correlations are treated in Refs. [4–6]. Convective boiling in subcooled water flowing through a heated channel is essential in many engineering applications, such as in the divertor plates of fusion reactors where peaches of about 20 MW/m^2 have to be removed [7]. The effects of surface orientation and gap size on the pool boiling heat transfer and critical hest flux (CHF) have been studied in Ref. [8]. However, the processes of nucleate boiling and, in particular, the boiling

* Corresponding author. Tel.: +39 05120 93292; fax: +39 05120 93296.
E-mail address: cesare.biserni@mail.ing.unibo.it (C. Biserni).

0017-9310/$ - see front matter © 2005 Elsevier Ltd. All rights reserved.
doi:10.1016/j.ijheatmasstransfer.2005.10.015

Nomenclature

dA	fractal or system dimension
dE	global embedding dimension
dL	local embedding dimension
d-Lyap	Lyapunov dimension, Eq. (1)
h	Lyapunov exponent
k	last exponent, Eq. (1)
n	order of the non-linear system, Eq. (4)
N	number of data on which $\phi_{\varepsilon\varepsilon}(t)$ is calculated
P	heating power, W
Q	mass flow rate, kg s^{-1}
t	time, s
$u(\blacksquare)$	input at the generic time sample, Eq. (2)
$x(t)$	time series measured on the system
$y(k)$	system outputs at a given instant k, Eq. (2)

Greek symbols

$\delta(t)$	distance between two trajectories at time t
$\varepsilon(t)$	normalised error
$\phi_{\varepsilon\varepsilon}(t)$	autocorrelation function of the normalised error
τ	time delay

Subscripts

0	referred to the initial time
i	ith element

crisis phenomenon, are quite complicated and a great number of uncertainties still remain.

The Vapotron effect [9–11] is a particular boiling process, firstly observed and named by Beutheret [9], that may occur as a consequence of the thermal interaction between a non-isothermal finned surface and a fluid locally subjected to a change of phase. This effect greatly enhances the heat exchange per unit area of the finned surface as the presence of fins, not only increases the heat exchange efficiency, but also contributes to stabilise the boiling process. In fact, a thermal gradient is formed along the fins so that the temperature at the fin base may exceed the boiling crises without endangering the system (unless Leidenfrost's temperature is exceeded). The technique initially adopted allowed for heat removal rates up to 1.5 MW/m^2; further developments (Supervapotron effect) were shown to be able to ensure values of 3 MW/m^2 (due to the stabilisation of the transition area). These values were then further exceeded by the Hypervapotron effect, able to remove up to 30 MW/m^2 [10], which was obtained through a closer disposition of the fins and in conditions of forced main subcooled flow.

The Vapotron effect and its "descendants" Supervapotron and Hypervapotron are characterised by the same cyclic repetition, for each cavity, of the three steps reported in Fig. 1 and described as follows:

(1) the coolant entrapped inside the cavities is heated until the saturation temperature is locally reached and vapour starts to form; at the same time the main flow outside the cavities is at a mainly constant subcooled state;
(2) the bubble grows until it fills the cavity and is expelled in the main flow in a very short transient;
(3) once in the main subcooled flow, the bubble collapses as a consequence of vapour condensation; at the same time subcooled fluid fills the cavity again.

The cyclic nature of the phenomenon, with rapid and transient phase changes, makes the study of the system dynamics fundamental also for the basic comprehension of involved thermodynamical aspects.

In this contest, for a deeper knowledge of the phenomenon, a wide series of operating conditions has been detected during an experimental campaign. In a preliminary study [12] it has been observed that the experimental time series are not periodic. Therefore, this paper aims at verifying whether the system is chaotic or not through the application of non-linear techniques to the analysis of experimental time series. The application of these techniques has allowed to show the chaotic nature of the Vapotron dynamics, similarly to what has been done in [13].

As a second step, the application of a non-linear identification strategy has been proposed in this study in order to define a non-linear predictive model of the system dynamics. The proposed approach is based on the application of Multilayer Perceptron neural networks for the generalisation of a NARMAX model, analogously to what has been done in [14,15] for the prediction of other complex thermal-fluidynamic systems.

2. Description of the experimental apparatus

A schematic representation of the experimental system is shown in Fig. 2. The main components of the experimental set up are:

- a polycarbonate test Section 1, allowing visual inspection;
- an electrically heated finned aluminium plate (2), having 32 fins 7 mm high, 3 mm thick and spaced 2 mm one from another;
- a hydraulic circuit with a circulation pump (5), a water tank (4), valves (6) regulating the coolant mass flow rate, a flow meter (3) measuring the flow rate and a heat exchanger for the cooling of the refrigerant fluid (7);
- a number of thermocouples and other auxiliary devices, among which a variac transformer controlling the heat power supply;
- an acquisition data system.

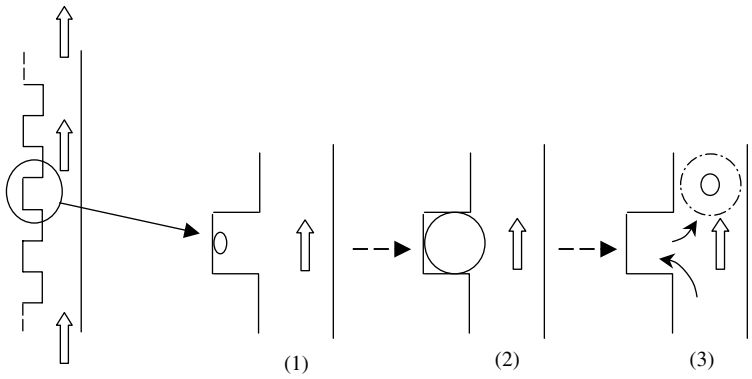

Fig. 1. Typical succession of events that a bubble experiences during the Vapotron phenomenon.

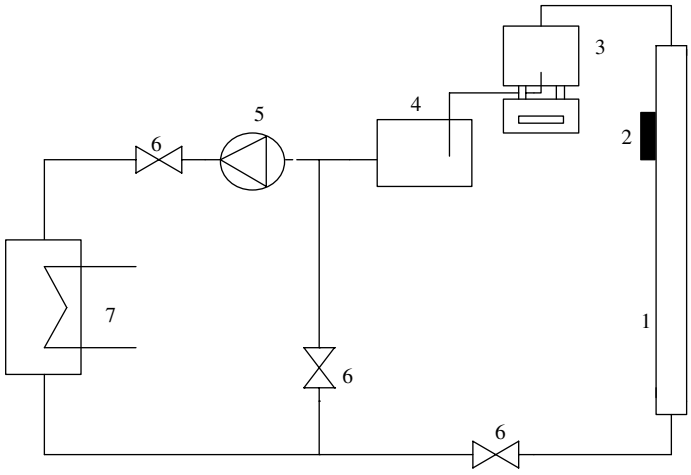

Fig. 2. Schematic of the experimental apparatus.

In the experimental campaign temperatures were measured through calibrated thermocouples (Type K chromel–alumel) with the error limits reported in Table 1, defined according to standard limits of error as published in IEC 584.

Radiation between the fins and the thermocouples has been neglected. The diameter of the tip of the thermocouples was 1 mm, in order to minimise the disturbances induced by the thermocouple on the dynamics of the phenomenon.

It is worth noting that the temperature measured in the lowest cavity is the only one not affected by the disturbances caused by vapour bubbles coming from the cavity placed below, whereas for the one placed at the middle of the heating surface several bubbles, coming from previous cavities, will affect the measure.

Table 1
K-type thermocouples error limits

Type of wire	Temperature range	Error limits
Type K chromel–alumel	−40 °C to 1000 °C	$\pm 0.004 \times t$, t = measured value

A set of experimental tests has been performed on this apparatus for various cooling mass flow rate and heating rate of the plate. These are the only input variables that have been allowed to vary during the experimental campaign; they are, in fact, the main variables characterising the system behaviour and influencing the dynamics of the Vapotron effect. Table 2 reports the operating conditions that have been tested during the experimental campaign for the various values considered (the heating power, P, and coolant mass flow rate, Q) in this study. Blank spaces correspond to the operating conditions for which the Vapotron effect has not been observed, i.e. for which the heat removal has been ensured by means of simple convection without the occurrence of phase changes.

Table 2
Experimental operating conditions

Mass flow rate Q (kg/s)	Heating power supplied to the finned plate, P (W)				
	1200	1300	1400	1500	1600
0.026	X	X	X	X	X
0.05			X	X	X
0.096				X	X

The time series of the temperature of the fluid inside the cavity and of the heated plate have been measured at different positions for each experimental test. In this study, the attention has been focused on the dynamical behaviour of the fluid temperature measured inside the lowest cavity, i.e. the first encountered by the flow, and inside one of the cavities at the centre of the heated plate, which have been addressed in the following respectively as $T1$ and $T2$.

Sampling at 36 kHz has been performed, though only the mean value of 900 data has been recorded. In this way it has been possible to remove high frequency noise components and to obtain an actual sampling rate of 40 Hz. This sampling rate had been demonstrated to be sufficient for a satisfactory representation of the system dynamics during preliminary tests. The length of each test has been set sufficiently wide to allow for the observation of the long-term regime behaviour of the system.

3. Non-linear analysis in the phase space: fundamentals

Recent efforts have been devoted to the exploitation of chaos, and hence of determinism, in boiling heat transfer phenomena of various kinds [16,17]. This is a step of primary importance in order to achieve a deeper knowledge of boiling dynamics and to choose appropriate modelling techniques. In fact, the study of chaotic systems requires the adoption of ad hoc analysis and modelling techniques.

It is worth reporting two main characteristics of a chaotic system [18–20]:

(a) after a relatively short time interval, very similar initial states produce very different dynamical states;
(b) if the temporal window of observation of a chaotic phenomenon is wide enough, recurrence can be manifested through the observation of a long term regular structure of the dynamics.

The first property explains the long-term unpredictability that characterises chaotic system and is usually addressed to as *strong dependence on initial conditions* [21]. The second property ensures that in the long term it is possible to observe recurrent behaviours. This implies that the behaviour observable in small time windows may be approximately repeated if the observation period is wide enough, even though such repetitions are not identical and occur in an irregular fashion. Recurrence is at the basis of the so-called *short-term predictability* [21], which allows for a fundamental distinction between chaotic behaviours and absolutely unpredictable stochastic behaviours. Moreover, it explains the typical non-periodic evolution of chaotic system and the consequent *broadband power spectrum*, often erroneously associated to noise or to the stochastic nature of the phenomenon [18].

This implies that FFT analysis is inadequate and different kind of representations are necessary to study chaotic behaviours, such as the representation in *phase space* or *state space* [18], spanned by an independent set of system variables. In this representation space, each point corresponds to a system state, whereas a trajectory is a series of system states and can be used to describe the dynamical evolution of the system. In the long term, the trajectory of the system generates in phase space a structure called *attractor* [19]. The geometrical properties of the attractor are fundamental to characterise the possible regimes of deterministic (i.e. not stochastic) systems. From a mathematical point of view, the phase space is a multidimensional orthogonal space that ensures that dynamically different pieces of trajectory (corresponding to different series of dynamical states) do not intersect with each other, in accordance with the *Theorem of Existence and Uniqueness* [21] that holds for deterministic systems. If noise does not affect the system, the occurrence of such intersections implies that different dynamical states are erroneously represented by the same point of the phase space [18], i.e. the dimension of the phase space must be increased.

The global embedding dimension, dE, corresponds to the minimum number of state variables necessary to obtain an unfolded representation (i.e. without undue intersections) of the attractor considered as a whole and is generally a priori unknown. Analogously, on a local basis it is possible to define the local embedding dimension, dL, i.e. the number of independent variables that are necessary, in the mean, to obtain an unfolded representation of smaller regions of the attractor (and hence $\mathrm{dE} \geqslant \mathrm{dL}$).

An analytical way to choose the correct dimension of the representation space is an application of Takens' method of delays [22], namely the *phase space reconstruction*. In particular, Takens' theorem demonstrates that if $x(t)$ is any time series measured on the system, it is possible to define an orthogonal space by choosing a set of (independent) time-delayed copies, $x(t), x(t+\tau_1), x(t+\tau_2), \ldots, x(t+\tau_n)$.

The correct number of state variables can be chosen through the evaluation of the rate of *unfolding* of the attractor. In fact, dynamically different pieces of trajectory are represented close to each other or lead to false intersections (*false neighbours*) [18] when the dimension of phase space is insufficient. With the growth of the phase space dimension, the number of false neighbours is progressively reduced until it becomes stable or grows again, when the optimal phase space dimension has been reached (corresponding to either dE or dL, depending on the window of observation of the analysis).

It is worth noting that the attractor unfolding depends also on the choice of the delays τ_i [18]. In fact, if the τ_i are too small, irrelevant differences exist between the time series and its delayed copies (i.e. the bases are not independent), whereas, if the τ_i are too high, the correlation between delayed copies is lost, together with the global structure of the attractor. The τ_i may be analytically chosen through the evaluation of the *average mutual information* [18]. Nonetheless, it is often possible to empirically perform this choice by checking the rate of unfolding of the attractor graphically represented in two or three dimensions.

Finally, the study of determinism of a dynamical system can be performed by evaluating the so-called *invariant characteristics* of the phase space representation of the system dynamics [18], i.e. properties of the system not depending on the chosen phase space. In particular, invariant characteristics allow for the classification of the system dynamics and can be calculated directly from experimental data through the creation of a phase space reconstructed from the experimental time series. The invariant characteristics considered in the present study are *fractal dimension* and *Lyapunov exponents* [18–21].

3.1. Fractal dimension

One of the most interesting invariant properties of a chaotic system describes the geometrical distribution of the attractor, typically characterised by fractal structure [21]. The main features characterising fractal structures are *self-similarity* and *lack of smoothness*. The former corresponds to the existence of inherent scale invariance, which means that after repeated amplification, fractal structures usually maintain the same geometrical appearance. The latter refers to the jagged or disconnected distributions shown by groups of trajectories, i.e. in a chaotic attractor there are often spatially separated layers of trajectories.

Both these properties are measured by the so-called *fractal* or *system dimension*, dA, which is fractional and greater than two for chaotic systems [18–21]. There is not a unique analytical definition of fractal dimension. The most common definitions are those of *capacity dimension*, *information dimension* and *correlation dimension* [21], but their evaluation is computationally intense and sensitive to noise in the experimental time series. An indirect approach for an estimation of dA is based on the *Embedding Theorem*, which in fact requires that $dE \geqslant 2dA + 1$. If the aim of the estimation of dA is limited to detect the existence of a possible chaotic behaviour ($dA > 2$), it can be sufficient to verify that dE is greater than five. Moreover, if $dE > dL$ a correspondence exists between dA and dL, i.e. dL is an integer greater than dA.

Finally, a convenient direct analytical approach to determine the fractal dimension consists in its evaluation on the basis of *Lyapunov exponents*.

3.2. Lyapunov exponents and Lyapunov dimension

The concept of global or local embedding dimension is connected to the existence of a corresponding number of directions along which the system dynamics evolves in phase space. Chaos theory associates to these directions a measure of the exponential tendency of two trajectories close to each other to converge or diverge. Considering for simplicity a one-dimensional system, i.e. evolving in one direction, if δ_0 is the distance between two trajectories at time t_0, the distance $\delta(t)$ at time t will be $\delta(t) = \delta_0 e^{ht}$. The exponent h is called *Lyapunov exponent* and strongly characterises the dynamic behaviour of the system [20]. The sign of this exponent is of primary importance, as it describes if the trajectories diverge ($h > 0$), converge ($h < 0$) or maintain the same distance ($h = 0$). For a generic system locally embedded in a dL-dimensional space, the knowledge of the dL Lyapunov exponents can be used to give a direct proof of the existence of chaos [20,21]. From a physical point of view, positive and negative Lyapunov exponents correspond to the existence of directions along which expansion and contraction of the attractor occurs, respectively. A chaotic system must have at least one positive Lyapunov exponent, i.e. one direction in which expansion occurs. Moreover, as a net contraction effect is required to ensure the global stability of the system, the sum of all Lyapunov exponents must be negative. On the basis of Lyapunov exponents it is possible to calculate the fractal dimension dA; the corresponding fractal dimension is called *Lyapunov dimension*, d-Lyap, and is defined by the following expression, according to Ref. [17]:

$$\text{d-Lyap} = k - \frac{\sum_{i=1}^{k} h_i}{h_{k+1}} \tag{1}$$

In Eq. (1), h_i denotes the ith Lyapunov exponent (ordered for decreasing value, from positive to negative) and k labels the last *exponents* for which $h_1 + h_2 + \cdots + h_k \geqslant 0$.

4. Analysis in phase space: results and discussion

This section describes the results of the phase space analysis performed on the experimental time series detected on the experimental system described in Section 2.

Fig. 3 shows the projections in a two-dimensional representation space of the attractors of time series detected by thermocouples $T1$ and $T2$ during two experimental tests characterised by the same coolant mass flow rate (0.026 kg/s) and by heat supply $P = 1200$ W and $P = 1400$ W respectively. These plots are in the overall well representative of the attractors of the experimental time series detected during the other operating conditions reported in Table 2. It is worth noting that, though complex, the attractors do have a well-defined structure, which hints at the existence of a deterministic source of the dynamics and excludes stochastic behaviours. In addition, the attractor shape strongly varies with the operating condition; moreover also the point of measurement plays a fundamental role on the morphology of the attractor. It is worth noting that the attractor of time series $T2$ is noisier than that of time series $T1$. This can be explained considering that $T2$ is measured in the cavity placed at the middle of the heating plate, whereas $T1$ is measured in the first cavity encountered by the flow and therefore is not affected by the disturbing effect of the bubbles released from lower cavities. Moreover, the attractor of $T2$ always occupies a wider region of phase space with respect to that of $T1$ and appears morphologically more complex, as a consequence of the faster dynamics of time series $T2$ with respect to $T1$, better described in [12]. Finally, it is important to

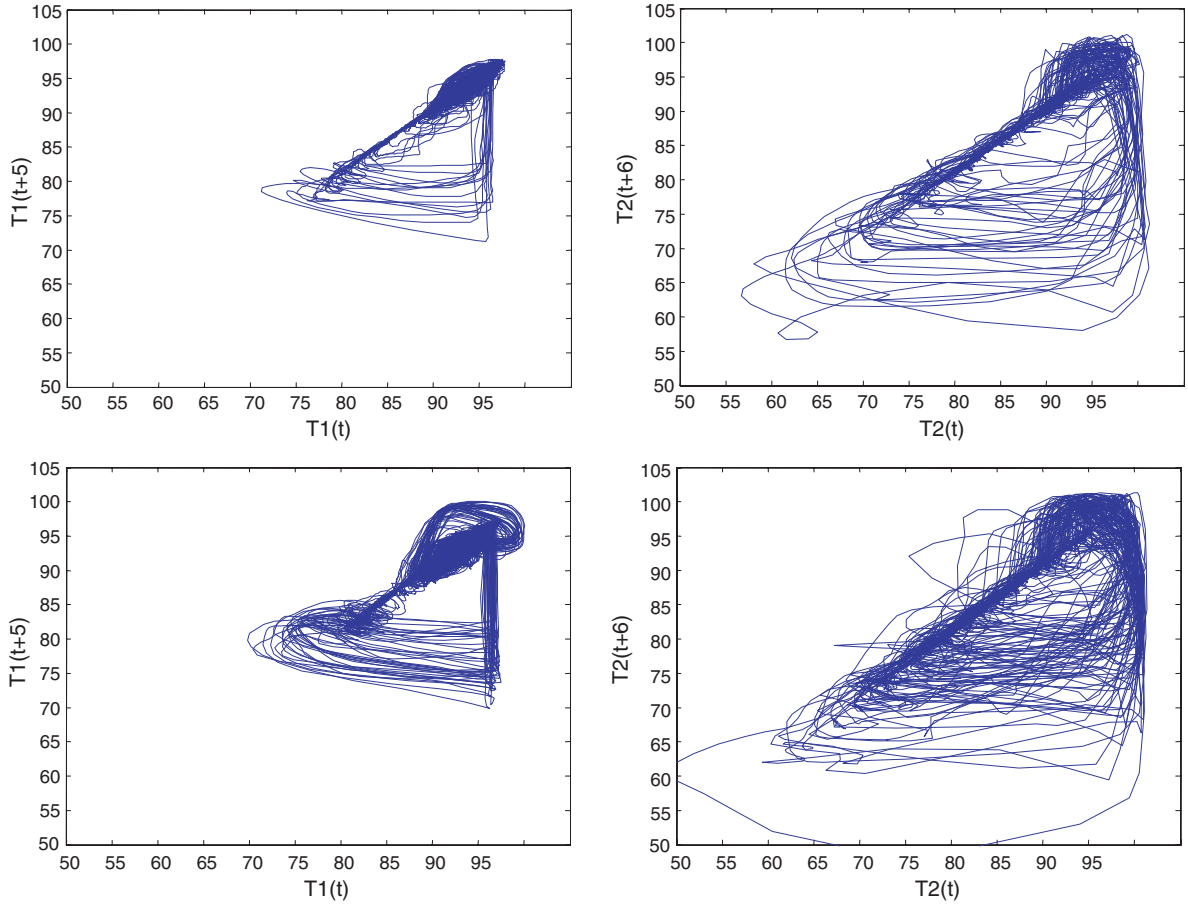

Fig. 3. Attractors of experimental time series $T1$ (on the left) and $T2$ (on the right) for the operating conditions characterised by $Q = 0.026$ kg/s and $P = 1200$ W (first row) and $P = 1400$ W (second row).

observe that the attractors present a fractal distribution, only in part depleted by the presence of measurement noise in the time series, which represents a strong indication of the existence of chaos in the system dynamics.

4.1. Embedding dimensions and Lyapunov dimension

Table 3 reports the values of global and local embedding dimensions, dE and dL, and of Lyapunov dimension d-Lyap, calculated for coolant mass flow rate $Q = 0.026$ kg/s and growing heat power supplied to the heating plate (first three rows of Table 3) and for heat power supplied to the heating plate $P = 1600$ W and growing coolant mass flow rate (last three rows of Table 3). Reported results refer only to time series $T2$ because of its faster dynamics, which has allowed results evaluation on a wider set of complete oscillations.

Table 3
Experimental time series $T2$, various operating conditions: calculated values of dE, dL and d-Lyap

Experimental test	dE	dL	d-Lyap
$Q = 0.026$ kg/s, $P = 1200$ W	8	6	5.57
$Q = 0.026$ kg/s, $P = 1400$ W	10	5	4.48
$Q = 0.026$ kg/s, $P = 1600$ W	8	6	5.76
$Q = 0.050$ kg/s, $P = 1600$ W	9	5	4.21
$Q = 0.096$ kg/s, $P = 1600$ W	10	6	5.64

Results reported in Table 3 show that the phase space reconstruction for the experimental time series $T2$ always requires a *global embedding dimension* not less than eight and *local dimension* not less than five. Moreover, Lyapunov dimension is always fractional and greater than two. These results demonstrate the existence of a chaotic source of the dynamics for the system under consideration. It is worth noting that d-Lyap is always a fraction comprised between dL and dL − 1, which was reasonably expected. On the other hand, in general it is not verified that $dE \geqslant 2dA + 1$, which is probably due to the influence of measurements noise in the experimental time series.

4.2. Lyapunov exponents

The values of the Lyapunov exponents calculated for time series $T2$ for the same operating condition discussed in Table 3 are reported in Table 4.

Reported Lyapunov spectra give another evidence of the existence of chaos. In particular, for all of the time series:

Table 4
Lyapunov spectra for experimental time series $T2$ under various operating conditions

	$Q = 0.026$ kg/s, $P = 1200$ W	$Q = 0.026$ kg/s, $P = 1400$ W	$Q = 0.026$ kg/s, $P = 1600$ W	$Q = 0.050$ kg/s, $P = 1600$ W	$Q = 0.096$ kg/s, $P = 1600$ W
L1	0.386	0.243	0.357	0.207	0.383
L2	0.253	0.161	0.222	0.088	0.236
L3	0.125	0.006	0.109	−0.004	0.120
L4	−0.002	−0.149	0.000	−0.152	−0.003
L5	−0.250	−0.696	−0.127	−0.630	−0.223
L6	−0.658		−0.686		−0.816
Sum	−0.156	−0.425	−0.125	−0.503	−0.303

(a) there are at least two positive Lyapunov exponents, i.e. there are two directions along which expansion of the attractor occurs; hence, the system must be addressed as hyper-chaotic;
(b) there are at least two negative Lyapunov exponents, which correspond to two directions along which contraction of the attractor occurs;
(c) one of the Lyapunov exponents is close to zero, confirming that the system is autonomous [19], i.e. the system dynamics is governed by an internal source and is not produced by an external forcing term;
(d) the sum of the whole set of Lyapunov exponents is negative, i.e. a net contraction effect dominates the system dynamics and ensures that the system is globally stable.

5. NARMAX model of the Vapotron effect

Results of previous analyses have underlined the intrinsic non-linear nature of the system dynamics. Therefore, the NARMAX (Non-linear Auto-Regressive Moving Average with eXogenous inputs) identification strategy has been chosen in order to define a proper non-linear model for the prediction of the system dynamics. In fact, the *NARMAX* model is a general class of non-linear input–output models able to provide a reliable description for a large class of non-linear systems [23]. In particular, the NARMAX strategy is based on the characterisation of the system outputs $y(k)$ at a given instant k, by means of the application of a non-linear map F to the inputs and outputs observed during previous time steps. Considering for simplicity a SISO (*single input–single output*) system, this means that $y(k)$ can be expressed as

$$y(k+1) = F[y(k), \ldots, y(k-n_y), u(k-1), \ldots, u(k-n_u)] \tag{2}$$

where $u(\blacksquare)$ is the input at the generic time sample.

In the present study the NARMAX approach has been generalised through the implementation with *Multilayer Perceptron neural networks*, which allow defining a unique model valid for different equilibria [24]. In this way the function F has been approximated by a neural network, NN, trained to map the output of the system in a wide range of its operation

$$y(k) \approx \mathrm{NN}[y(k-1), \ldots, y(k-n_y), u(k-1), \ldots, u(k-n_u)] \tag{3}$$

In particular, a family of neural network has been trained to reproduce the dynamics of the temperature oscillations that characterise the Vapotron effect. The structure of this family of neural networks has been chosen in accordance with the following basic consideration on the physical process:

- the mass flow rate of the coolant, Q, and the heat supplied at the finned surface, P, are the inputs to the system and completely define each operating condition;
- among the measured system outputs, the application of the NARMAX model has been limited to the temperature measured inside the lowest cavity, $T1$.

Adapting the general formula (3) to the present case, the input–output relation defining the model can be expressed as

$$[T1(k+1)] = \mathrm{NN}[T1(k), T1(k-1), \ldots, T1(k-n), Q, P] \tag{4}$$

where n, represents the order of the non-linear system (which is a priori unknown).

A preliminary consideration is necessary in order to justify the approach adopted in this study for the creation of the training set for the neural model. In fact, the demonstration of the chaotic behaviour of the system in study reported in the previous section authorises to form training set by selecting a few pieces of experimental time series $T1$ (three pieces in the present study), for each of the fifteen operating conditions reported in Table 2. The choice of these pieces is performed with the aim of achieving a satisfactory representation of some of the dynamics manifested by the system during the particular operating condition. Nonetheless, due the chaotic nature of the system under consideration, these the selected pieces of the time series cannot be exhaustive of the infinite set of possible dynamics of the system.

A main advantage offered by the generalised NARMAX approach is that, if the creation of the training set is performed properly, after the training phase the neural network should be able to satisfactorily predict any of

the possible dynamics of temperature $T1$ within the range of the system operations considered during the training.

The prediction capabilities of the neural model have been verified during a testing phase. This phase is performed using a new set, namely testing set, which is much wider than the training set and does not contain the pieces of time series of the latter. In the present study, for simplicity the testing set has been created considering the whole set of time series $T1$ detected during all the operating conditions, but eliminating the pieces used for the creation of the training set, in order to ensure that the evaluation of the model performances is performed properly (i.e. on the prediction of "unknown" dynamics).

The determination of the optimal order of the model and of the optimal number of hidden neurons has been performed by means of a heuristic approach. In order to choose the optimal value of n it is possible to evaluate the properties of the errors that affect the prediction of the outputs of models of different order, which can be defined as the differences between experimental and simulated time series. In general, the characteristics of the error are considered satisfactory when the error behaves as *white noise*, i.e. it has zero mean is uncorrelated [20]. In fact, satisfaction of both these requirements implies that the neural network has *captured* the deterministic part of the system dynamics, which are therefore accurately modelled. To this aim, it is necessary to verify that the autocorrelation function of the normalised error $\varepsilon(t)$, namely $\phi_{\varepsilon\varepsilon}(t)$, assumes the values 1 for $t = 0$ and 0 elsewhere, i.e. it behaves as an impulse. This is indeed an ideal condition and, in practice, it is sufficient to verify that $\phi_{\varepsilon\varepsilon}(t)$ remains in a confidence band usually fixed at the 95%, which means that $\phi_{\varepsilon\varepsilon}(t)$ must remain inside the range $\pm 1.96/\sqrt{N}$, with N number of data on which $\phi_{\varepsilon\varepsilon}(t)$ is calculated [25].

Fig. 4 reports the autocorrelation function calculated during the testing phase for growing model orders, considering the same piece of time series, detected during operating condition characterised by coolant mass flow rate $Q = 0.026$ kg/s and heat power supply $P = 1500$ W. The first plot in Fig. 4 refers to the best neural network model for $n = 1$ (obtained with a neural network with 15 hidden neurons) and its analysis shows that the autocorrelation function overcomes the prescribed limits. The same happens for the second plot in Fig. 4, which refers to the best neural network model for $n = 3$ (obtained with a neural network with 10 hidden neurons). Finally the last plot of Fig. 4 reports the satisfactorily autocorrelation function obtained with the best neural model for $n = 5$, corresponding to the neural network with 15 hidden neurons.

The previous analysis has been confirmed during the testing phase of the whole range of operating conditions. In particular, for all of the operating conditions, the analysis of the autocorrelation function of the error for increasing model order (from $n = 1$ to 6) has pointed out $n = 5$ as the optimal value. In fact, as in Fig. 4, the increase of the order until $n = 5$ progressively reduced the autocorrelation of the error, whereas further increases appeared not only to be ineffective but even to slightly deteriorate the autocorrelation properties. The first plot in Fig. 5 shows the comparison of the experimental time series (full line) versus the simulation of the fifth order NARMAX model (dashed line) for the operating condition characterised by coolant mass flow rate $Q = 0.026$ kg/s and heat power supply $P = 1500$ W. The analysis of this plot allows to perceive the satisfactorily performances of the model in the prediction of the experimental time series. It is remarkable that the model is able to reproduce all of the different complex patterns shown by the time series. In particular, it is able to accurately predict not only the "slow" dynamical patterns that occurs at high temperature (during the growth of the vapour bubble inside the cavity), but also the "fast" burst towards lower temperatures that occur when the vapour bubble is ejected in the subcooled main flow and subcooled fluid refills the cavity. The second plot in Fig. 5 reports the prediction error of the model, corresponding to the same experimental and simulated time series reported in the upper plot. Also this diagram evidences that the neural network predictions are satisfactory, producing a maximum error of about 0.5 °C, which, moreover, corresponds to the fastest dynamical behaviour observed in the time series, i.e. the worst condition for prediction. It is worth noting, in fact, that the maximum error in the second plot of Fig. 5 occurs when the time series in the upper plot experiences an abrupt decrease of more than 30 °C in less than 60 steps, i.e. less than 1.5 s. Results obtained during the testing of the fifth order neural network in the whole range of

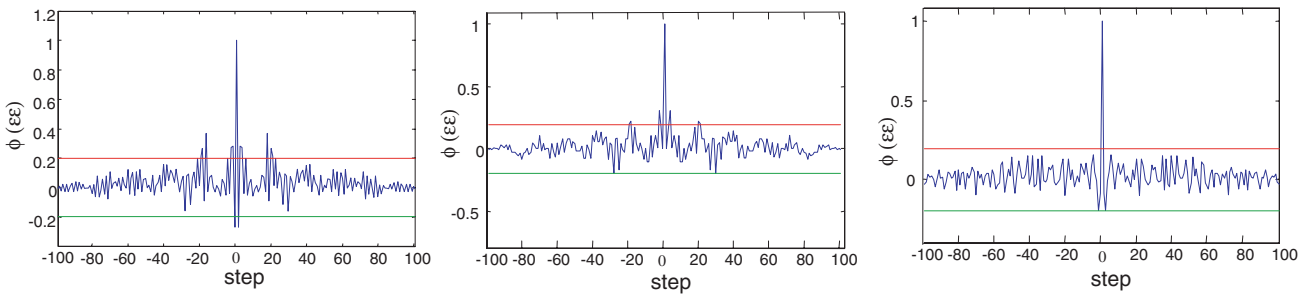

Fig. 4. Autocorrelation of the testing error for models of order $n = 1$ (first plot), $n = 3$ (second plot) and $n = 5$ (third plot). Condition $Q = 0.026$ kg/s and $P = 1500$ W.

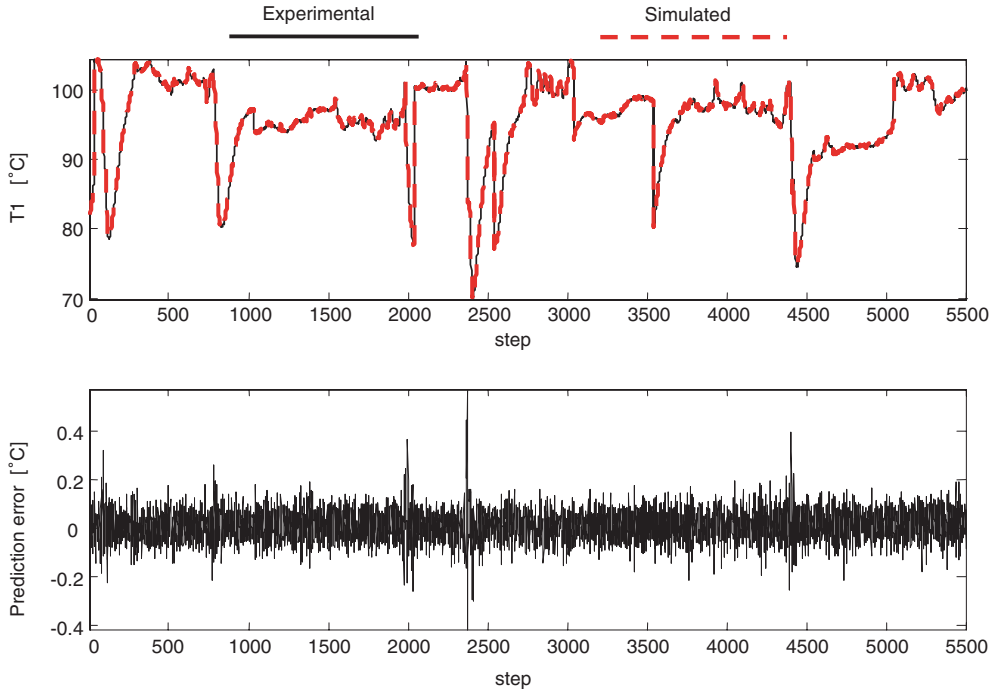

Fig. 5. NARMAX model performances. First plot: comparison of the experimental time series $T1$ (operating condition $Q = 0.026$ kg/s and $P = 1500$ W) and the corresponding simulation of the fifth order NARMAX model. Second plot: corresponding prediction error of the model.

operating conditions detected during the experimental campaign are perfectly consistent with those reported so far, for $Q = 0.026$ kg/s and $P = 1500$ W. In other words, the model proposed for short-terms prediction of the complex thermal-fluidynamic behaviours arising in Vapotron presents satisfactory performances in the whole range of operation considered in this study.

6. Concluding remarks

An innovative approach has been proposed for the analysis and modelling of the complex dynamics that arise in the subcooled boiling heat transfer phenomena that characterises an experimental Vapotron system.

In the first part of the study, the application of non-linear time series analyses to the experimental dynamics has lead to the demonstration of the chaotic nature of the dynamical phenomena. This result has been deduced through both the observation of a complex but regular structure of the attractors of the experimental time series and the analytical evaluation of chaotic invariant characteristics of the attractors. In particular, calculation of global and local embedding dimensions, Lyapunov dimension and Lyapunov spectra have analytically proved the existence of a chaotic source of the dynamics. This means that the system is non-linear and deterministic, i.e. it is possible to define only short-term predictive models. To this aim, in the second part of this study the experimental time series have been used in order to define a non-linear input–output identification model, based on the NARMAX approach. The strategy has been implemented and generalised by means of Multilayer Perceptron neural networks, trained to predict the experimental time series of the temperature measured in the first cavity of the heated finned surface in which Vapotron phenomenon takes place. Reported results show that the model is able to give satisfactory predictions of the experimental time series and that the chosen neural network methodology is able to perform correct predictions in the whole range of operating conditions of interest.

Acknowledgements

The Authors wish to thank the Italian MIUR for supporting the research.

References

[1] A. Bejan, Shape and Structure, from Engineering to Nature, Cambridge University Press, Cambridge, UK, 2000.
[2] G.P. Peterson, A. Ortega, Thermal control of electronic equipment and devices, Adv. Heat Transfer 20 (1990) 181–314.
[3] F. Inasaka, H. Nariai, Evaluation of subcooled critical heat flux correlations for tubes with and without internal twisted tapes, Nucl. Eng. Des. 163 (1996) 225–239.
[4] H. Sakashita, T. Kumada, Method for predicting curves of saturated nucleate boiling, Int. J. Heat Mass Transfer 44 (2001) 673–682.
[5] M.A. Islam, M. Monde, Y. Mitsutake, CFC characteristics and correlations of concentric-tube open thermosyphon working with R22, Int. J. Heat Mass Transfer 48 (2005) 4615–4622.
[6] T. Okawa, A. Kotami, I. Kataoka, M. Naitoh, Prediction of the critical hest flux in annular regime in various vertical channels, Int. J. Heat Mass Transfer 229 (2004) 223–236.
[7] F.J. Collado, Critical hest flux thermodynamics, Nucl. Eng. Des. 61–62 (2002) 165–170.

[8] Y.H. Kim, K.Y. Suh, One-dimensional critical heat flux concerning surface orientation and gap size effects, Nucl. Eng. Des. 226 (2003) 277–292.
[9] C. Beutheret, Transfert de flux superieur a 1 kW/cm^2 par double changement de phase entre une paroi non isotherme et une liquide en convection forces, in: Proc. Int. Heat Transfer Conf., Paris, 1970.
[10] G. Cattadori, G.P. Gaspari, G.P. Celata, M. Cumo, A. Mariani, G. Zummo, Hypervapotron technique in subcooled flow boiling CHF, Exp. Therm. Fluid Sci. 7 (1993) 230–240.
[11] G. Lorenzini, C. Biserni, A Vapotron effect application for electronic equipment cooling, ASME J. Electr. Pack. 125 (2003) 475–479.
[12] C. Biserni, A. Fichera, E. Lorenzini, A. Pagano, Experimental analysis of the dynamics of a system exhibiting Vapotron effect, in: Proc. 13th Int. Conf. on Thermal Eng. and Thermogrammetry, Budapest, Hungary, June 2003, pp. 412–420.
[13] A. Fichera, C. Losenno, A. Pagano, Experimental analysis of thermo-acoustic combustion instability, Appl. Energy 70 (2) (2001) 179–191.
[14] A. Fichera, A. Pagano, Neural network-based prediction of the oscillating behaviour of a closed loop thermosyphon, Int. J. Heat Mass Transfer 45 (2002) 3875–3884.
[15] L. Cammarata, A. Fichera, A. Pagano, Neural prediction of combustion instability, Appl. Energy 72 (2) (2002) 513–528.
[16] M. Shoji, Y. Takagi, Bubbling features from a single artificial cavity, Int. J. Heat Mass Transfer 44 (2001) 2763–2776.
[17] L.H. Chai, M. Shoji, Boiling curves—bifurcation and catastrophe, Technical Note in Int. J. Heat Mass Transfer 44 (2001) 4175–4179.
[18] H.D.I. Abarbanel, Analysis of Observed Chaotic Data, Institute for Non-Linear Science, San Diego, 1995.
[19] J.M.T. Thompson, H.B. Stewart, Nonlinear Dynamics and Chaos, John Wiley & Sons, New York, 1986.
[20] S.N. Rasband, Chaotic Dynamics of Nonlinear Systems, John Wiley & Sons, New York, 1990.
[21] Y.A. Kuznetsov, Elements of Applied Bifurcation Theory, second ed. Applied Mathematical Sciences, vol. 112, Springer-Verlag, New York, 1998.
[22] F. Takens, in: D.A. Rand, L.S. Young (Eds.), Lecture Notes in Mathematics, Dynamical System and Turbulence, Springer, New York, 1981.
[23] S. Chen, S.A. Billings, P.M. Grant, Representations of non-linear system: the NARMAX model, Int. J. Control 49 (5) (1989) 1013–1032.
[24] I.J. Leontaritis, S.A. Billings, Input–output parametric models for nonlinear systems, Part I: deterministic non-linear systems, Int. J. Control 41 (2) (1985) 303–328.
[25] S.A. Billings, H.B. Jamaluddin, S. Chen, Correlation based model validity tests for nonlinear models, Int. J. Control 44 (1986) 235–244.